https://doi.org/10.5194/egusphere-2024-835
Preprint. Discussion started: 18 April 2024

Tracing rate and extent of human induced hypoxia during the last 200 years in the mesotrophic lake Tiefer See (NE Germany)

Ido Sirota[1*], Rik Tjallingii[1], Sylvia Pinkerneil[1], Birgit Schroeder[1], Marlen Albert[1], Rebecca Kearny[1], Oliver Heiri[2], Simona Breu[2] and Achim Brauer[1,3]

[1]Section Climate Dynamics and Landscape Evolution, GFZ German Research Centre for Geosciences, Potsdam, Germany

[2]Geoecology, Department of Environmental Sciences, University of Basel, Basel, Switzerland

[3]Institute of Geosciences, University of Potsdam, Potsdam, Germany

*Corresponding author: Ido Sirota (idosir@gfz-potsdam.de)

https://doi.org/10.5194/egusphere-2024-835
Preprint. Discussion started: 18 April 2024

Abstract. The global spread of lake hypoxia, [O_2] < 2 mg/l, during the last two centuries has a severe impact on ecological systems and sedimentation processes. While the occurance of hypoxia was observed in many lakes, a detailed quantification of hypoxia spread remained largely unquantified. We track the evolution of hypoxia and its controls during the past 200 yrs in lake Tiefer See (TSK; NE Germany) using 17 gravity cores, recovered between 10 and 62 m water depth in combination with lake monitoring data. Lake hypoxia was associated by the onset of varve preservation in the TSK, and has been dated by varve counting to 1918±1 at 62 m water depth and reached a lake-floor depth of 16 m at 1997±1. This indicates oxygen concentration to fell below the threshold for varve preservation at the lakefloor (>16 m). Sediment cores at 10-12 m depth do not contain varves indicating well oxygenation of the upper water column. Monitoring data show that the threshold for hypoxia at the depocenter is a period of five months of [O_2] < 5 $\frac{mg}{l}$ and two months of [O_2] < 2 $\frac{mg}{l}$. Detailed TOC, $\delta^{13}C_{org}$ and XRF core scanning analyses of the short cores indicate that the depletion in DO started several decades prior to the varve preservation. This proves a change in the depositional conditions in the lake following a transition phase of several decades during which varve preservation was not accomplished. Furthermore, varve preservation does occur at seasonal stratification and not necessarily requires permanent stratification.

Keywords: Hypoxia, Lake sediments, Varves, XRF core scanning, environmental monitoring

1 Introduction

The vertical distribution of dissolved oxygen (DO) in lakes and shallow marine environments is among the most important factors regulating the ecology, biogenic and chemical conditions, primary sedimentation and diagenesis of sediments in such environments (Diaz & Rosenberg, 1995; Dräger et al., 2017; Nürnberg, 2004; O'Reilly et al., 2015; Shatkay et al., 1993; Tyson & Pearson, 1991; Wetzel, 2001). The development of hypoxic conditions in lakes, [O_2] < 2 mg/l (Nürnberg, 2004; Tyson & Pearson, 1991; Vaquer-Sunyer & Duarte, 2008), during the last ~200 years is a threat for ecological and sedimentary systems. It is driven by both natural and anthropogenic processes (Diaz & Rosenberg, 2008; Jenny et al., 2016), such as climate warming (Jankowski et al., 2006; Meire et al., 2013; Njiru et al., 2012), enhanced water column stratification and decreased lake circulation (Jankowski et al., 2006; Straile et al., 2003), nutrient input increasing primary productivity and decomposition of organic matter (Dräger et al., 2017; Kienel et al., 2013), and water-sediment interactions (Steinsberger et al., 2017). Hypoxic conditions in lakes support the burial and preservation of organic matter (OM) in lacustrine records (Arthur & Dean, 1998; Dräger et al., 2017). The burial of OM in lacustrine sediments has a substantial contribution to the global carbon fixation, and it is estimated to reach half the carbon fixation in the oceans (Dean & Gorham, 1998; Kastowski et al., 2011; Mendonça et al., 2017; Mulholland & Elwood, 1982; Tranvik et al., 2009), due to the high OM productivity in lakes (Tyson & Pearson, 1991), and the high burial efficiency under hypoxic conditions (Sobek et al., 2009). Thus, an accurate and high-resolution quantification of the rate and intensity of hypoxia spread in lakes and a good evaluation of OM productivity, accumulation and preservation in lake sediments are required.

https://doi.org/10.5194/egusphere-2024-835
Preprint. Discussion started: 18 April 2024

Over the years, attempts to reconstruct past oxygen level (paleo-redox conditions) in lakes used diverse sedimentological, geochemical and biological proxies (Anderson & Dean, 1988; Buatois et al., 2020; Dräger et al., 2019; Dräger et al., 2017; Friedrich et al., 2014; Jenny et al., 2013; Makri et al., 2021; Ojala et al., 2000; Sorrel et al., 2021; Teranes & Bernasconi, 2005; Ursenbacher et al., 2020). Laminae preservation along lacustrine successions indicates the absence of bioturbation organisms, while non-laminated intervals reflect DO level sufficient for the existence of bioturbation organisms (Diaz & Rosenberg, 1995; Friedrich et al., 2014; Jenny et al., 2013; Kelts & Hsü, 1978; Kienel et al., 2013; Ojala et al., 2000; Schaffner et al., 1992; Tylmann et al., 2012; Tyson & Pearson, 1991; Zolitschka et al., 2015). Limited oxygen availability for laminated sediment intervals is further supported by high bulk sediment TOC concentrations within these sediments due to the reduced organic matter (OM) decomposition (Arthur & Dean, 1998; Diaz & Rosenberg, 1995; Dräger et al., 2017). OM degradation results in selective degradation of organic compounds with a more negative $\delta^{13}C$ composition and explains the more negative $\delta^{13}C_{org}$ values measured in laminated sediments (Benner et al., 1987; Dräger et al., 2017; Lehmann et al., 2002; Mollenhauer & Eglinton, 2007; Spiker & Hatcher, 1987). Therefore, $\delta^{13}C_{org}$ analyses allow to determine whether high TOC concentrations increased production or preservation. An additional method for reconstructing oxygen level in lakes is X-ray fluorescence (XRF) scans of sediment cores (Evans et al., 2019; Makri et al., 2021; Sanchini et al., 2020; Sorrel et al., 2021; Zander et al., 2021). The element data allow a continuous and high-resolution reconstruction of paleo-redox conditions, rather than the binary laminated non-laminated perspective. Specifically, the ratio between Fe and Mn ratio is often used for paleo-redox reconstructions because of the differential re-mobilization of Fe and Mn under redox conditions (He et al., 2023; Loizeau et al., 2001; Makri et al., 2020; Makri et al., 2021; Żarczyński et al., 2019), although the Fe/Mn ratio remains a proxy of relative changes of the sediment redox state. The abundance of oxygen-sensitive bioturbating organisms in lakes was used for DO level reconstruction (e.g., Ursenbacher et al., 2020). In temperate regions, chironomid species during their larval stage serve as one of the main bioturbating organisms in lakes. Remains of these larvae preserve well in the sediments and their analysis therefore potentially allows reconstructions of past DO concentrations as well and to link the spread of hypoxic conditions to laminated intervals (Brodersen et al., 2004; Davies, 1976; Heinis & Davids, 1993; Ursenbacher et al., 2020). However, the abovementioned methods commonly were applied on a single sediment core from the deepest part of the lake basin, so that the rate of the spatiotemporal spread of hypoxia remained unknown. In this study, we apply a multi-proxy approach on multiple sediment cores from the entire lake basin at different water depths.

Annually laminated or varved lake sediments are unique high-resolution archives to reconstruct the intensity of hypoxia and evaluate the rate in which hypoxic conditions spread (Dräger et al., 2019). Reconstructing the rate and extent of hypoxia in mesotrophic lakes provides a valuable basis for sustainable development, biological conservation and evaluating anthropogenic pressure on the environment (Jenny et al., 2016; Njiru et al., 2012). This study addresses open questions on the spatiotemporal evolution of hypoxia within a lake and critical conditions for initiating preservation of varved sediments. The objectives of this study are to, (i) reconstruct the spatiotemporal spread of hypoxia in Tiefer See during the last two centuries in detail, (ii) decipher the rate of hypoxia spread in lake TSK and the response of the sedimentary system to depleted DO levels, (iii) explore the drivers for hypoxia development and identifying thresholds for hypoxia spread in the lake. Finally, we want to

https://doi.org/10.5194/egusphere-2024-835
Preprint. Discussion started: 18 April 2024

test the common approach of using varve preservation as proxy for a hypoxic lake regime. Our approach combines micro-facial and geochemical analyses of 17 gravity sediment cores from different water depths and locations within the lake basin with lake water monitoring data. The results are supported by palaeoecological analyses (subfossil chironomids) from selected samples of two of the cores to support the interpretation of changing DO levels at these sites.

2 Site description

The Tiefer See (TSK; 53º 35.50'N, 12º31.80'E; 62 m a.s.l) is located in the northeastern German lowlands (Figure 1A) and part of the Klocksin lake chain, and was formed within a subglacial channel system at the end of the last glaciation. It has an elongated axis oriented north-south with steep slopes on the east-west directions (Figure 1B) and has a surface area of 0.75 km^2. The modern lake has a maximum depth of 62 m and is an ideal site to link environmental conditions to the preservation of laminated sediments (Roeser et al., 2021). The lake has relatively wide and shallow margins (Figure 1C) and the deepest part of the lake (31-62 m) includes only small part of the lake's area (~16 %) and water volume (~10 %). Only negligible inflow enters the lake directly from lake Flacher See and the small catchment area (~5.2 km^2) is dominated by glacial till of the terminal moraine. This area is presently used as arable land, whereas the lake shorelines are covered by a narrow band of large alder, ash, and oak trees (Kienel et al., 2013).

The TSK is a mesotrophic-monomictic lake with a stratified water column from March to October, while the water column is well mixed from November to February (Roeser et al., 2021). This limnologic mode has a significant impact on lake's circulation, oxygenation of the water column and endogenic mineral formation. Present-day annually laminated sedimentation comprises an early spring diatom sub-layer, a late spring-early summer endogenic calcite sub-layer (Kienel et al., 2017; Roeser et al., 2021), and an autumn-winter mixed layer of organic matter and littoral calcite sub-layer (Roeser et al., 2021). The three layers closely follow the annual stratification and oxygenation of the lake with thermal stratification strengthening during spring and summer and a well-mixed water column during autumn and winter. Allogenic sedimentation, such as dust influx and sediment transport by surface runoff is negligible.

The TSK Holocene sediment record is characterized by frequent alternations between varved and homogeneous non-varved intervals (Dräger et al., 2019; Dräger et al., 2017). Varved intervals are associated with high TOC content of ~15%, while sediments of non-varved intervals characterized by a lower TOC content of ~5% (Dräger et al., 2019). The preservation of varved interval is attributed to the prevailing hypoxic conditions (Dräger et al., 2017), and indicate that the TSK is sensitive to various processes that regulate oxygen levels along the water column.

https://doi.org/10.5194/egusphere-2024-835
Preprint. Discussion started: 18 April 2024

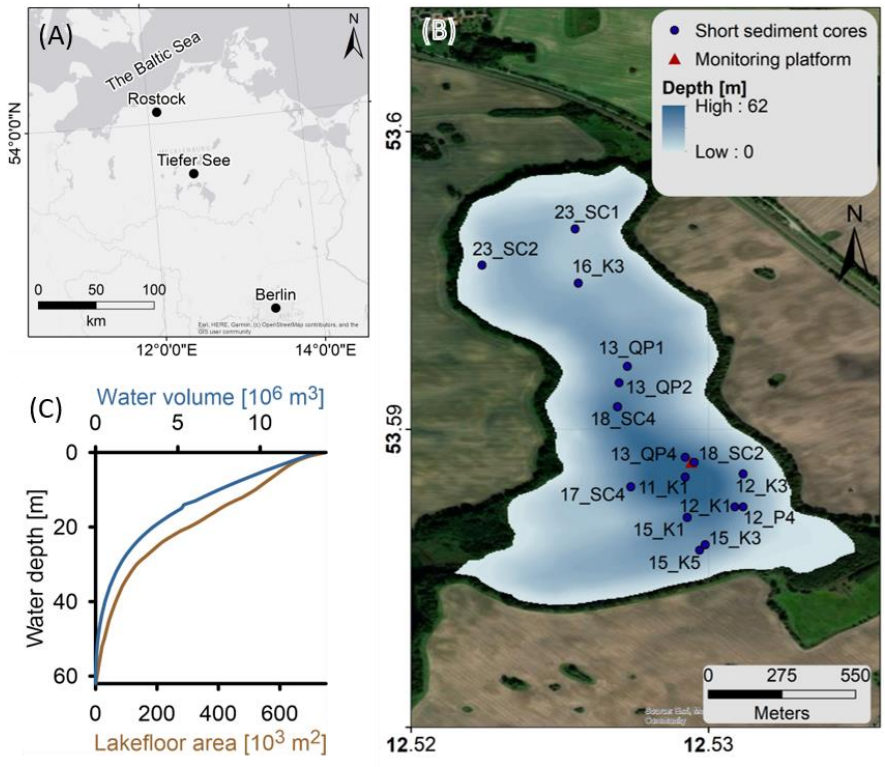

Figure 1: Location map of the TSK. (A) The lake is located at the Southern Baltic region, and it is located at a subglacial channel system. (B) TSK bathymetry, short cores and monitoring system locations. (C) The hypsometric curve of the lake. Imagery photo source: ESRI, Earthstar Geographics, and the GIS user community.

3 Methods and materials

In this study we apply a novel combination of two independent high-resolution proxies for hypoxia; (i) varve preservation and counting based on microfacies analyses that provides a very good time constrain, and (ii) high resolution geochemical depth profiles that allow to quantify the spread of hypoxia in the lake. (iii) Faunal remains as indicators for potential burrowing organisms. This combination is applied for sediment cores from different water depths and locations within the lake basin (Figure 1). For selected cores and intervals, we also analyzed the remains of chironmid larvae in the sediments, one of the main bioturbating organism groups in TSK that is expected to change in abundance and species composition with changing DO. In order to quantify present-day seasonal variations in hypoxia, we use lake water monitoring data.

3.1 Sediment cores

In total 17 short cores were taken with a 90 – mm UWITEC gravity corer (Dräger et al., 2019) during the period of 2011-2023 at different locations and water depths, between 10-62 m (Figure 1), covering the recent varved

https://doi.org/10.5194/egusphere-2024-835
Preprint. Discussion started: 18 April 2024

interval in the lake. Each one of the cores is documented by the location, water depth [m], core length [cm] and thin section length [cm]. After recovery, the cores were left settling in a cold room for two weeks in a vertical position at a temperature of 4°C before core opening and sampling (Roeser et al., 2021).

3.2 Micro-facies analyses

From 16 of the cores, 46 overlapping thin sections (100 x 25 mm) were prepared following the standard procedure for soft sediments based on the freeze-drying technique and impregnation with epoxy resin (Brauer & Casanova, 2001). For an overview, thin sections were first scanned on a standard flatbed scanner with 1200 dpi resolution. Detailed microfacies analyses was carried out using two different types of microscopes, a Zeiss Axio–Zoom V16 and an Olympus DP72 with non-polarized, semi-polarized and polarized light. For each core, a composite profile of series of overlapping thin sections was established by microscopic correlation. Varve counting was carried out on these continuous thin section profiles for each gravity core.

3.3 Chronology

The chronology of the cores is based on three methods, (i) varve counting, (ii) core correlation by marker layers, and (iii) tephrochronology.

3.3.1 Varve counting, marker layers identification and core correlation

We adopt the varve facies model from Roeser et al. (2021) for varve counting in large scale (10 cm long) thin sections using a petrographic microscope. Marker layers (ML) are distinct layers or sequences of laminae that can be identified in several cores and serve for core correlation. ML are considered as isochrons and their age is determined by varve counting. ML definition was done on core TSK11-K1 due to its excellent recovery and its location in the deepest part of the lake (Figure 1), with a single ML that was identified in core TSK18-SC4 that allows to complete the varve counting until 2018, thus covering the entire recent hypoxic period.

3.3.2 Tephrochronology

Tephrochronology was applied for three cores from intermediate water depths (TSK12-K1 from 35.1 m; TSK13-QP1 water depth 30.3 m; TSK15-K5 water depth 27.3 m) to identify the Askja (Iceland) eruption from CE 1875 as an independent isochrone. Previous work by Wulf et al. (2016) has identified the Askja-1875 as a crypto-tephra layer in the core TSK11-K1. From each of the cores in this study, five continuous 1-cm-interval samples were analyzed from the age-depth interval which is expected to include the Askja-1875 tephra. The extraction of these microscopic glass shards from the sediment samples used the adapted methods outlined in Blockley et al. (2005). The volcanic glass shards were then identified via microscopy before being physically extracted using the method outlined in Lane et al. (2014). The major and minor elemental composition of the individual shards were measured using electron probe microanalysis (EPMA) using the JOEL JXA-8230 at GFZ Potsdam. The operating conditions were as followed: a beam size of 5-10µm with 15kV voltage and a 10 nA beam current. The count times for Fe, Ti, Mg, Mn, Cl and P were 20 s and for Si, Al, K, Ca and Na were 10 s. The machine was calibrated using the glass standards of MPI-Ding glasses ATHO-G, StHs-6-80 and GOR-132-

https://doi.org/10.5194/egusphere-2024-835
Preprint. Discussion started: 18 April 2024

G (Jochum et al., 2006) and Lipari obsidian (Hunt & Hill, 1996) with measurements taken on these glasses during the run to ensure precision and accuracy.

3.4 Geochemical sediment characterization

3.4.1 XRF scanning

Micro-XRF scanning maps were measured on impregnated sediment blocks, which are the residual counter part of the thin-sections. The XRF element maps allow direct comparison of the geochemical composition and thin-section observations of individual layers. Elemental XRF mapping analyses were performed in a vacuum chamber at 50 µm resolution with a Bruker M4 Tornado micro-XRF scanner. This micro-XRF scanner is equipped with a Rh X-ray source that is operated at 50 kV and 0.60 mA. The poly-capillary X-ray optics produces a high intensity irradiation spot of about 20 µm that allows fast measurement times of 50 ms.

Continuous element records were acquired every 0.2 mm directly at the split core surface using an ITRAX XRF core scanner, which is equipped with a Rh X-ray source (30 kV, 60 mA). These non-destructive analyses were performed for 4 s after removal of the oxidized surface sediments and covering the core surface with XRF-transparent foil. Element intensity records (in cps) were acquired for the elements Si, S, K, Ca, Ti, Mn, Fe, and Sr, which contain information of the relative element concentration, but are also influenced by changes of physical sediment properties and matrix absorption and enhancement effects (Tjallingii et al., 2007). However, log-ratios of element intensities are free of physical and matrix effects, and also allow consistent statistical analysis of compositional data (Weltje et al., 2015).

Geochemical characterization and element correlations records of the XRF scanning records have been further explored using Ward's hierarchical clustering and principal component analysis (PCA). The statistical analyses were performed center-log-ratio transformed element intensities of the elements mentioned above for all sediment cores to reveal similarities and differences for all sediments within the lake system.

3.4.2 TOC, $\delta^{13}C_{org}$ and $CaCO_3$ determination

Five short cores (TSK11-K1, TSK12-K1, TSK13-QP1, TSK15-K5 and TSK23-SC2) were sampled for the purpose of determining TOC, $\delta^{13}C_{org}$ and $CaCO_3$ profiles at contiguous 1 cm^3 samples.

Total carbon (TC), total organic carbon (TOC) and $\delta^{13}C_{org}$ were determined using an elemental analyzer (FlashEA 1112) connected with a ConFloIV interface on a DELTA V IRMS (isotope ratio mass spectrometer, ThermoFischer Scientific) at the GeoForschungsZentrum Section 4.3 in Potsdam, Germany. For TC up to 2 mg sample material was loaded into tin capsules and burned in the elemental analyzer. The calibration was performed using Urea and checked with a soil reference sample (Boden3, HEKATECH). The TOC contents and $\delta^{13}C_{org}$ values were determined on in-situ decalcified samples. Around 3 mg of sample material were weighted into Ag-capsules, dropped first with 3 % and second with 20% HCl, heated for 3 h at 75°C, and finally wrapped and measured as described above. The calibration was performed using elemental (Urea) and certified isotope standards (IAEA-CH-7) and checked with internal reference sample. The isotopic composition is given in delta

https://doi.org/10.5194/egusphere-2024-835
Preprint. Discussion started: 18 April 2024

notation relative to a standard: δ (‰) = [(R_{sample} – $R_{standard}$)/$R_{standard}$)] x 1000 and the reproducibility for replicate analyses is 0.2 % for TOC and 0.2‰ for $\delta^{13}C_{org}$. Calcite contents were calculated by obtaining the total inorganic carbon content (TIC = TC – TOC) and multiplying by 8.33, which is the fraction molar mass of inorganic carbon from the $CaCO_3$.

3.5 Chironomid analysis

Abundance and taxonomic composition of chironomid remains were analyzed for selected subsamples from varved and non-varved sediment sections in two sediment cores, the shallow TSK15-K5 (27.3 m) and the deep TSK18-SC4 (61.1 m). Six sediment samples were analyzed in each core, with 2 cm³ of sediment processed for all samples except the deepest sample in core TSK-K5, where only 1 cm³ was analyzed. Three samples were taken from the top varved unit and three from the non-varved unit below. Sediments were washed through a 100-µm sieve and the sieve residue then examined under a stereomicroscope at 20-40x magnification using a Bogorov counting tray. Chironomid remains were sorted from other remains, mounted in Euparal mounting medium and identified at 100-400x magnification under a compound microscope. The remains were identified to morphotypes according to Brooks et al. (2007). Larval remains were classified into taxa that can colonize deepwater (profundal) environments in lakes and taxa restricted to shallow water (littoral environments) based on Brooks et al. (2007), Wiederholm (1983) and Saether (1979). Concentrations were calculated by dividing chironomid counts by the analyzed sediment volume and influx values by multiplying concentrations with estimated sediment accumulation rates in cm/yr. Interpretations focus on the overall concentrations, percentage abundances and influx values of the sum of profundal chironomids and selected profundal chironomid taxa.

3.6 Monitoring data

An observational setup based on a research platform at the deepest part of the lake used for high-resolution limnological-sedimentological monitoring since 2012 and provides that data used in this study (Roeser et al., 2021). Temperature and oxygen profiles of the water column were measured every 12 hr with an automatic water probe (YSI 6600 V2, Yellow Springs United States). This data is used to trace the evolution of the summer thermal stratification and variations in the scalar field along the water column. $CaCO_3$ and TOC contents, and $\delta^{13}C_{org}$ of modern sediments were measured on bi-weekly sediment samples collected by a sediment trap at a water depth of 50 m. The sediment sampling was conducted at intervals of 15 days with an automated sequential trap (Technicap PPS 3/3; active area 0.125 m^2) equipped with 12 sample bottles.

4 Results

4.1 Cores stratigraphy

15 cores retrieved from a water depth >12 m contain the uppermost varved interval (Figure 2). Two cores retrieved from less than 12 m water depth (TSK23-SC1/SC2) do not contain a varved unit. Except the two cores without a varved unit all cores depict a similar sediment sequence consisting of three units: The basal Unit B composed of homogeneous dark brown sediments is overlain by Unit G of homogenous grayish sediments

https://doi.org/10.5194/egusphere-2024-835
Preprint. Discussion started: 18 April 2024

followed by the varved Unit V on top. The thickness of Unit V ranges between 4.5 cm in the shallowest core (TSK16-K3) from 16 m water depth, and 40 cm in the deepest core (TSK11-K1) from 62 m water depth. In contrast, Unit G is thicker in the shallow water cores (13-15 cm) than in the depocentral cores (2 cm).

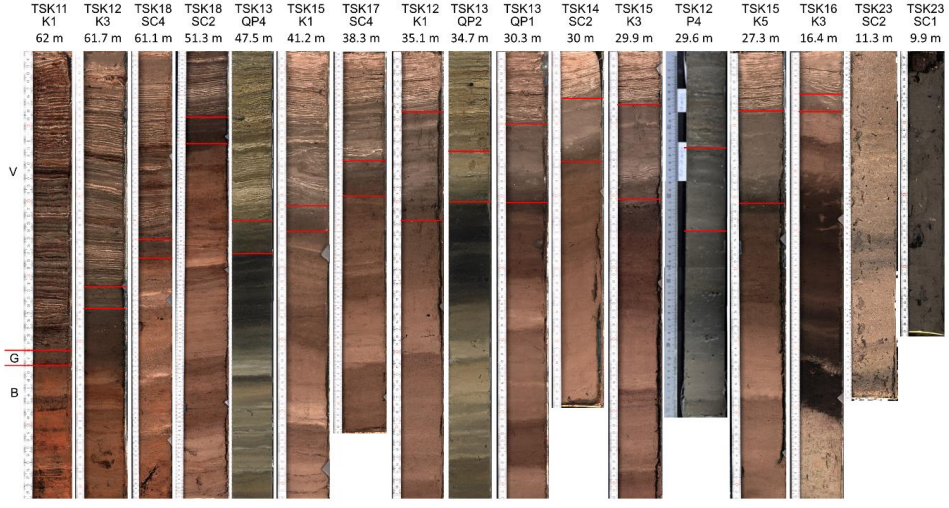

Figure 2. Core images of all short cores used in this study arranged form deep to shallow. V – varved unit at the top of each core, G – gray unit, B – brown unit.

4.2 Varve composition

The upper laminated unit is mainly composed of biogenic-calcareous varves as defined in the lake by Roeser et al. (2021) as triplet of diatom-rich, calcite-rich and resuspension sub-layers (Figure 3). Micro-XRF maps display the abundance of Ca and Si, as indicators for the calcite and diatom layers. They show that these elements concentrate along distinct laminae, emphasizing the seasonal deposition of calcite and diatoms. While the diatom and calcite sub-layers are very distinct in the Micro-XRF scans due to the high abundance of Ca and Si, the mixed layer is rich in organic materials with only minor calcite crystals and diatom frustules, and thus less distinct. The biogenic-calcareous varve type is deposited and preserved both at the deep and the shallow regions of the lakefloor (Figure 3).

https://doi.org/10.5194/egusphere-2024-835
Preprint. Discussion started: 18 April 2024

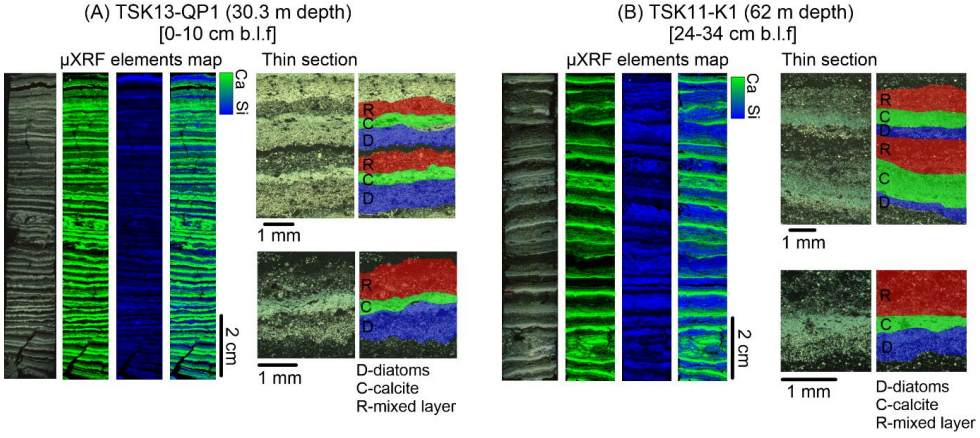

Figure 3. Typical varves in the Tiefer See displayed by thin section images and micro-XRF maps of Ca and Si display. (a) a shallow core, (B) a deep core.

4.3 Core chronology

The cores were dated by three methods, (i) varve counting, (ii) core correlation by marker layers, and (iii) tephrochronology. Varve counting and core correlation were applied on 14 cores to determine the age of the onset of varve preservation. The age of the boundary between units B and G has been obtained for four cores (TSK11-K1, TSK12-K1, TSK13-QP1 and TSK15-K5) by tephrochronology.

4.3.1 Chronology of the varved sediments (Unit V)

Varve counting and marker layers - TSK11-K1 master core. Core TSK11-K1 (obtained in 2011) has been selected as a master core where ten marker layers (ML1 -ML10) were defined and varve dated (Figure 4, Supplementary material table S1). In addition, ML0 formed in 2011 was identified in core TSK18-SC4 that has been obtained in 2018, seven years after core TSK11-K1. ML0 is the anchor point of the varve chronology with varves between 2011 and 2018 counted in core TSK18-SC4 and older varves in core TSK11-K1. Varve counting in core TSK11-K1 yields a total of 93±1 varves, thus dates the onset of varve preservation to CE 1918±1 yr.

Core correlation. The onset of varve preservation was independently established in all cores and confirmed by the marker layers (Figure 5, supplementary material Figure S1). In addition to the master core, two cores, TSK12-K3 and TSK18-SC4, are also located in the deepest part of the lake, at water depths of 61-62 m. A local event layer, triggered by a thunderstorm in 2011, and occurring in core TSK18-SC4, serves as an additional marker layer (ML0) with a known age. The onset of varve preservation in the deepest part of the lake in these cores is independently obtained by microscopic varve counting at CE 1923±1 (TSK12-K3) and CE 1919±1 (TSK18-SC4), thus, within the uncertainty of the onset of varve preservation in TSK11-K1 (CE 1918±1) and an earlier published age (Dräger et al., 2019). From the deepest part of the lake towards shallower depths, the onset

https://doi.org/10.5194/egusphere-2024-835
Preprint. Discussion started: 18 April 2024

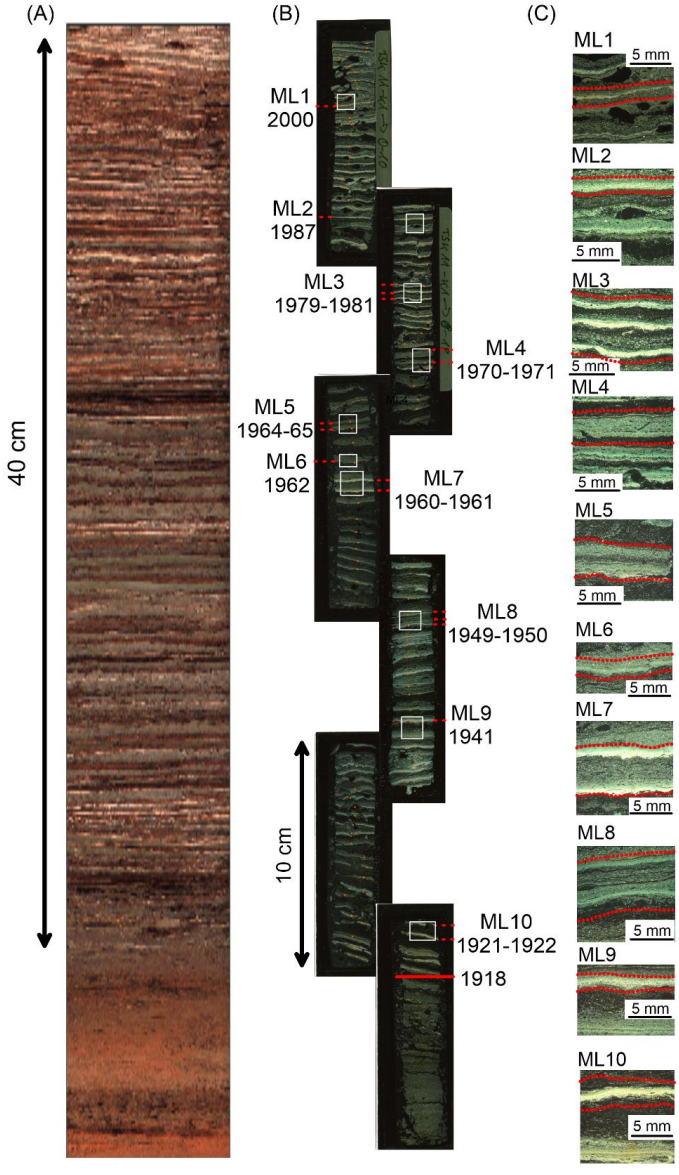

Figure 4. TSK11-K1 master core. (A) Image of the core. (B) Thin sections of the core. (C) Marker layers (ML).

of varve preservation becomes progressively younger (Figure 6, and Table 1). The onset of varve preservation at
275 TSK18-SC2 (51.3 m depth) was dated to CE 1925±1, at TSK15-K1 (41.2 m depth) to CE 1943±1, at TSK14-SC2 (30 m depth) to CE 1973±1 and at the shallowest core site, TSK16-K3 (16.4 m depth) the onset of varve preservation was dated to CE 1997±1. No varves were identified in the top sediments of the shallowest two cores, TSK23-SC1 and TSK23-SC2, from water depths of 10-12 m.

https://doi.org/10.5194/egusphere-2024-835
Preprint. Discussion started: 18 April 2024

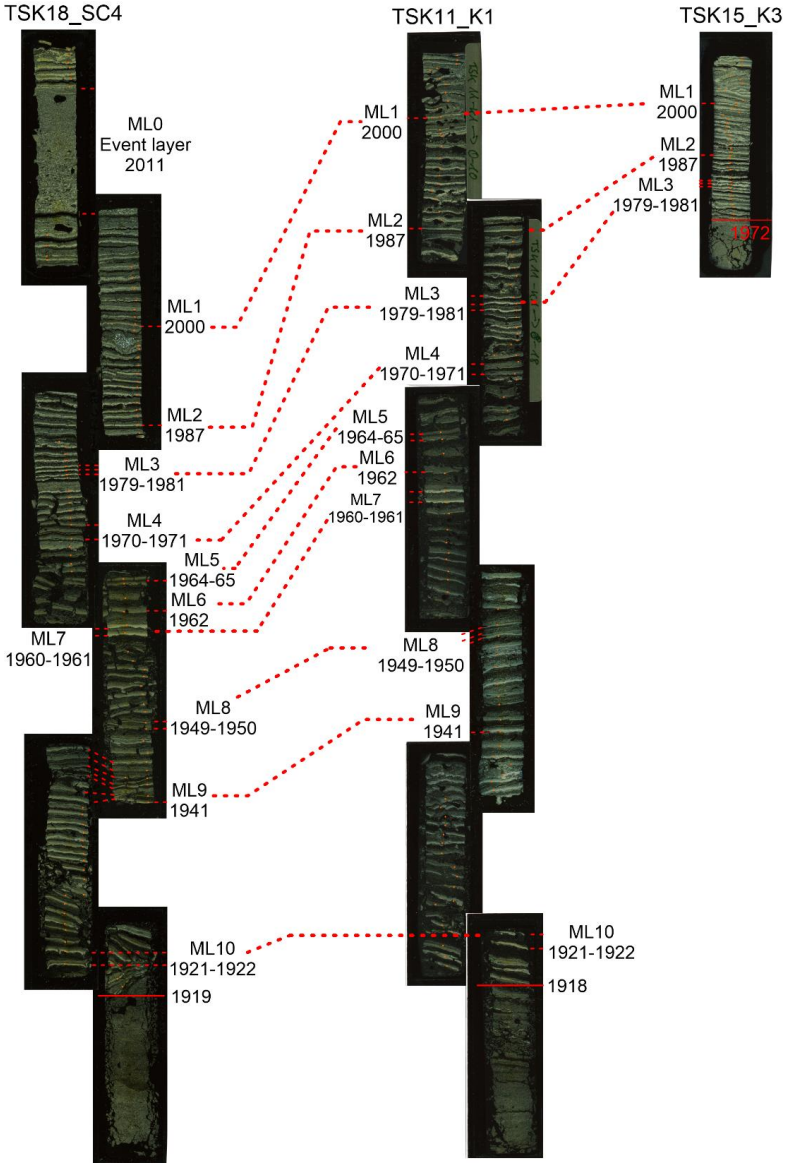

280 **Figure 5. Chrono-stratigraphic correlations between cores TSK18-SC4 and TSK15-K3 and the master core – TSK11-K1.**

4.3.2 Chronology of non-varved sediments (Units B and G)

The chronology of the non-varved sediments (Units B and G) was established by tephrochronology in four cores (TSK12-K1, TSK13-QP1 and TSK15-K5; additional age was taken for core TSK11-K1 from Wulf et al. (2016).
285 In each core, a peak in shard concentration was recognized and determined as isochron. Geochemical

https://doi.org/10.5194/egusphere-2024-835
Preprint. Discussion started: 18 April 2024

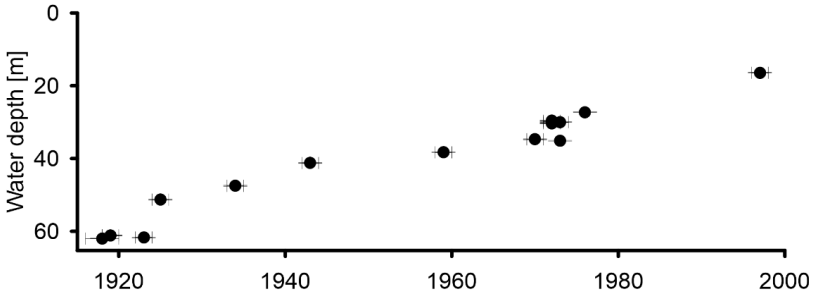

Figure 6. Spatiotemporal spread of hypoxia in Lake TSK as shown by the onset of varve preservation and recovery depth.

Table 1. List of all cores that were used in the study and the age of the base of the recent varved interval.

	Water depth	Location	Length of varved interval [cm]	Varve onset [yr CE]
TSK11-K1	62	N 53°35'35.60" E 12°31'48.00"	40	1918±1
TSK12-K3	61.7	N 53°35'36.00" E 12°31'49.00"	32.5	1923±1
TSK18-SC4	61.1	N 53°35'569" E 12°31'819"	36	1919±1
TSK18-SC2	51.3	N 53°35'623" E 12°31'818"	23	1925±1
TSK13-QP4	47.5	N 53°35'38.00" E 12°31'48.00"	24	1934±1
TSK15-K1	41.2	N 53°35'512" E 12°31'804"	21	1943±1
TSK17-SC4	38.3	N 53°35'574" E 12°31'690"	19	1959±1
TSK12-K1	35.1	N 53°35'32.00" E 12°31'54.00"	7.5	1973
TSK13-QP2	34.7	N 53°35'47.00" E 12°31'40.00"	10	1972±1
TSK13-QP1	30.3	N 53°35'49.00" E 12°31'41.00"	10	1970±1
TSK14-SC2	30		7	1973±1
TSK15-K3	29.9	N 53°35'457" E 12°31'840"	8	1972±1
TSK12-P4	29.6	N 53°35'32.00" E 12°31'55.00"	12	1972±1
TSK15-K5	27.3	N 53°35'446" E 12°31'829"	8.5	1976±1
TSK16-K3	16.4	N 53°35'984" E 12°31'584"	3.5	1997±1
TSK23-SC1	9.9	N 53°36'5.6154" E 12°31'34.68"	0	-
TSK23-SC2	11.3	N 53°36'1.224" E 12°31'23.412"	0	-

https://doi.org/10.5194/egusphere-2024-835
Preprint. Discussion started: 18 April 2024

compositions show that these volcanic shards originated from the Askja-1875 CE eruption. The volcanic glass shards were found in cores TSK13-QP1 and TSK15-K5 at the boundary between Units B and G, thus the age of this boundary is 1875. In core TSK12-K1 the shards were found 3 cm below this boundary and in core TSK11-K1 they were found 6 cm below Unit B and Unit G boundary, thus the age was estimated according to the average deposition rate of the sediments between the base of the varved unit and the identified tephra. As the crypto-tephra samples were undertaken at 1 cm that represents a certain time frame depending on the deposition rate at each core, a chronological error was added to the analysis.

4.4 Geochemical characterization

4.4.1 XRF cluster analysis

Statistical analyses were performed after center-log-ratio transformation of the element intensities of Si, S, K, Ca, Ti, Mn, Fe, and Sr for all 13 sediment cores to reveal similarities and differences for all sediments within the lake system. Five groups of similar geochemical composition were defined using Ward's hierarchical clustering. Element correlations and cluster analysis are shown in a PCA-biplot of PC1 and PC2 (Figure 7), which shows a clear divide between elements associated with detrital sediments (Ti, K), authigenic minerals (Ca, Si), and redox sensitive elements (Fe, Mn). Each data point is assigned to one of the five clusters and show the difference between oxidized sediment (1-3) and varved sediments (4-5).

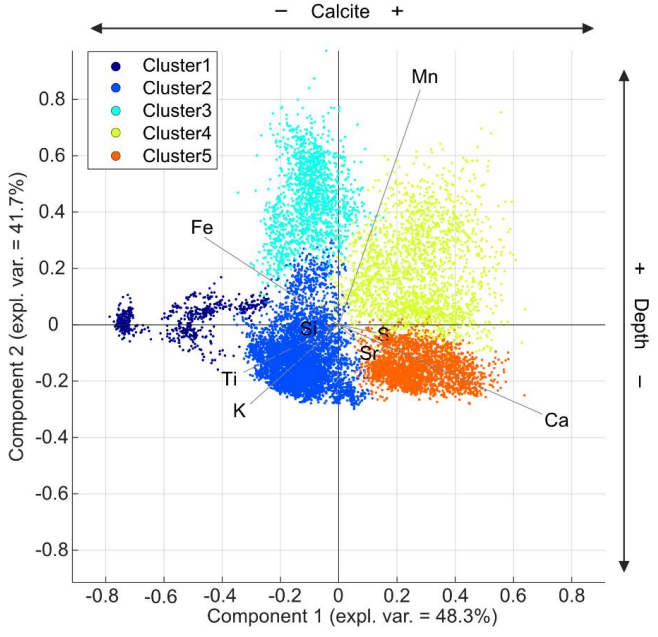

Figure 7. A biplot showing PC1 and PC2. All data points are classified into five clusters reflecting the different sediment types.

https://doi.org/10.5194/egusphere-2024-835
Preprint. Discussion started: 18 April 2024

Down-core cluster representations of the data points can be used for geochemical characterization of the different sediment types, and reveal a clear change from oxic sediments of Unit B to hypoxic sediments of Units G and V (Figure 8). Besides, the clustering results divide between cores from shallow locations of 11-41 m water depth and cores from the depocenter, from at 51-62 m water depth. For the deeper cores, Unit B is classified as cluster 3 while the upper Units G and V are classified as cluster 4. For more shallow cores, unit B is classified as cluster 2 while the upper Units G and V are classified as cluster 5. However, for all cores the change from Unit B to the upper Units G and V is mainly related with the increasing dominance of Ca (Figure 8). In all of the cores, except of TSK23-SC2, the transition from unit B to unit G is correlated with a substantial change in the geochemistry of the sediments marked by a transition between cluster 2 and cluster 5 (shallow cores) or between cluster 3 to cluster 4 (deep cores). Cluster 1 appears only in one core, TSK16-K3, and it reflects the glacial till.

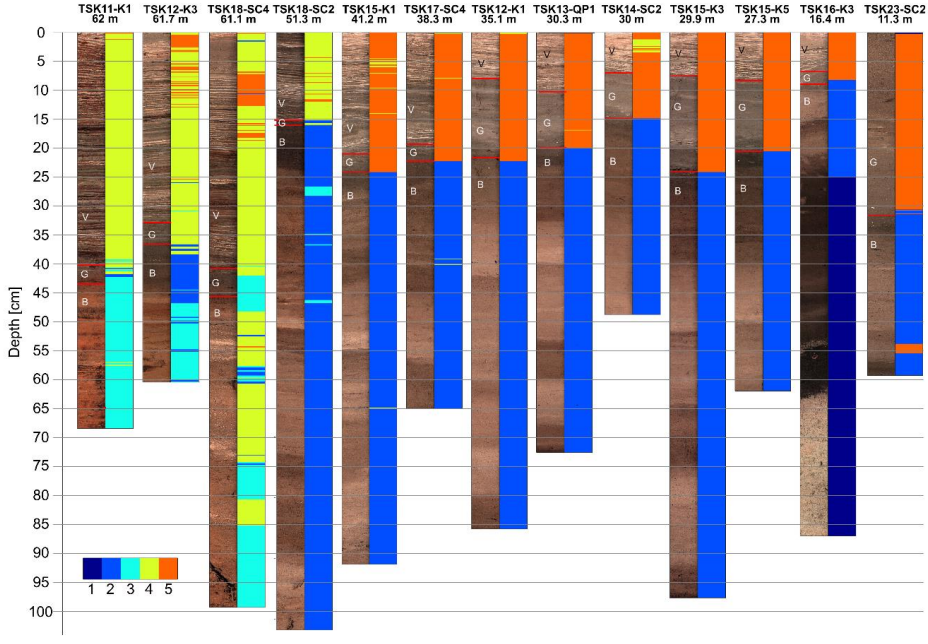

Figure 8. XRF stratigraphy of the cores. The colors of the clusters represent the geochemical classification of the sediments based on the cluster analysis presented in Figure 7. B - brown unit. G – gray unit. V – varved unit.

4.4.2 Geochemical sediment core profiles

Three cores, from different water depths (TSK11-K1 from 62 m, TSK15-K5 from 27.3 m and TSK23-SC2 from 11.3 m) were selected for detailed TOC, $\delta^{13}C_{org}$ and $CaCO_3$ analyses, and are presented here with XRF Ca/Ti, Si/Ti and Fe/Mn ratios (Figure 9). In core **TSK11-K1** (62 m) (Figure 9A), $CaCO_3$ content along Unit B ranges between 17-41% with an average of 28%, and it increases along the thin Unit G and the varved unit to 25-62% with an average of 44%. The TOC content moderately increases from ~3% at the bottom of the core to 11% at

https://doi.org/10.5194/egusphere-2024-835
Preprint. Discussion started: 18 April 2024

its top with no abrupt changes at the transition from Unit B to Unit G and at the transition to the varved Unit V. $\delta^{13}C_{org}$ values decrease from ~-28‰ at the bottom of the core to ~3-1‰ at the top of the core. While the change in TOC content upcore is moderate, a stepwise increase and a stepwise decrease is observed in $CaCO_3$ content and the $\delta^{13}C_{org}$ values respectively. Both roughly coincide with the transition from Unit B to Units G and V. The abrupt changes in $CaCO_3$ content and the $\delta^{13}C_{org}$ composition are coincided with changes in the XRF elemental ratios. Ca/Ti and Si/Ti ratios are both low along Unit B and they are substantially higher in the varved Unit. The Fe/Mn ratio displays a stepwise decrease at the transition from Unit B to Units G and V.

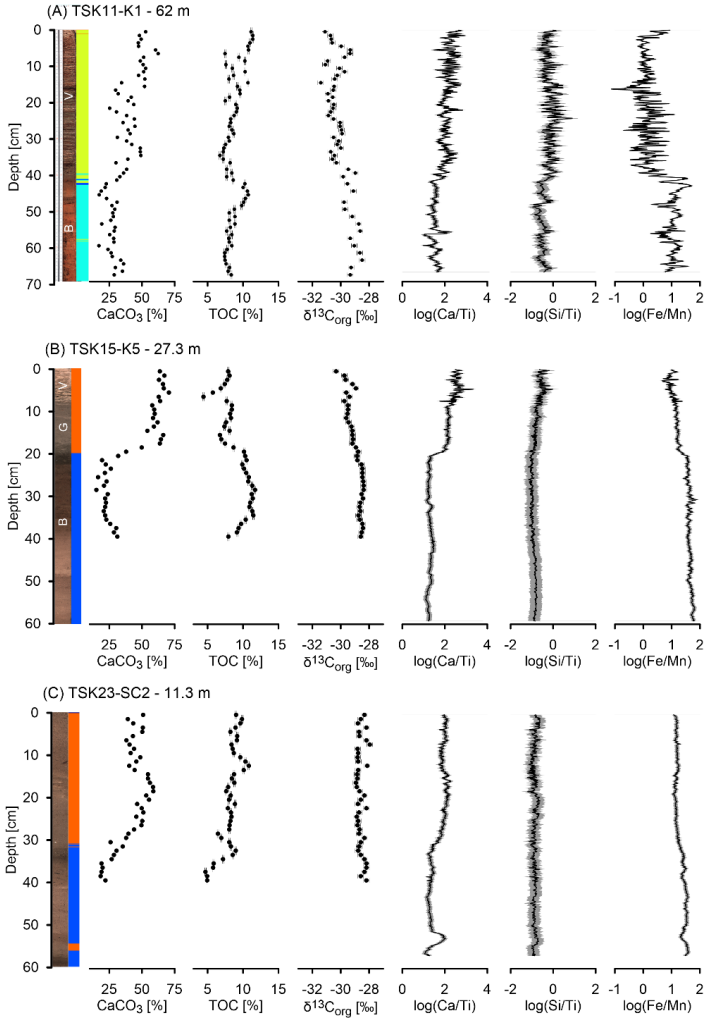

Figure 9. Core image, XRF stratigraphy, CaCO3, TOC, $\delta^{13}C_{org}$, Ca/Ti, Si/Ti, Fe/Mn, profiles of three cores from different water depths. (A) TSK11-K1 at 62 m depth, (B) TSK15-K5 at 27.3 m depth, and (C) TSK23-SC2 from 11.3 m depth.

https://doi.org/10.5194/egusphere-2024-835
Preprint. Discussion started: 18 April 2024

In core **TSK15-K5** (27.3 m) (Figure 9B), $CaCO_3$ content ranges from ~20% along Unit B to ~60% in the Units G and V. This abrupt increase appears at the transition from the cluster 2 to the cluster 5. The TOC content decreases from ~10% at Unit B to ~6% along Units G and V. $\delta^{13}C_{OM}$ values decrease from ~-28‰ at the bottom of the core to ~-30‰ at the top of the core. Both display a moderate change upcore in contrast to the abrupt change in $CaCO_3$ content. Ca/Ti and Si/Ti ratios are both low along Unit B and they are substantially higher along Units G and V. The Ca/Ti ratio displays a stepwise increase, which is correlated with the transition between units, while the Si/Ti ratio is moderately increase upward from that point. The Fe/Mn ratio decreases sharply from the transition between Unit B to Units G and V upcore.

In core **TSK23-SC2** (11.3 m) (Figure 9C), the changes in all proxies are less distinct. $CaCO_3$ content ranges from ~20% at the base of the core to ~50% at its upper part. This increase is roughly correlated with the transition between cluster 2 and cluster 5. The TOC content increases from ~5% in cluster 2 to ~10% along cluster 5. $\delta^{13}C_{org}$ values remain constant along the core within a narrow range of -28‰ to -28.8‰, and do not show a depletion trend like the other two cores. The Ca/Ti ratio is low at the base and it is moderately increasing from the transition between the cluster 2 to cluster 5. The Si/Ti ratio do not show a clear trend upcore. The Fe/Mn ratio is constant along the core with little variance. In contrast to the other two deeper cores, the transition between the clusters (and sediment units) is not associated with a change in the Fe/Mn ratio.

4.4.3 Chironomid abundance

Remains of chironomid larvae were present at low abundances in the analyzed cores, with the exception of the lowest sample in the intermediate water core (TSK15-K5) (Figure 10; full dataset in supplementary material Table S2). The assemblages were characterized by a high percentage of littoral (shallow-water) taxa remains, whereas profundal (deep-water) chironomids were only present at relatively low percentages. This is typical of sediments deposited under hypoxic or anoxic conditions, as the overall number of deep-water chironomids, close to the coring site, is reduced and a considerable amount of the larval remains are redeposited from shallower parts of the lake (Brodersen & Quinlan, 2006; Van Hardenbroek et al., 2011). At ~27 m water depth (TSK15-K5), the abundance, concentration and influx of remains of chironomid larvae are gradually reduced from Unit B to Unit G, and drop down to almost zero in Unit V (Figure 10A). In Unit B, high abundance of chironomids from profundal environments is observed, including high abundances of *Micropsectra radialis-type*, while in Unit G lower abundance of chironomids and M. radialis-type are observed and in Unit V only negligible amounts of chironomids are observed. In the deep-water core (TSK18-SC4), the overall abundance of chironomids and the abundance of profundal chironomids is very low throughout the core (Figure 10B), in line with low oxygen concentration and low amounts of bioturbation. However, among the most abundant deepwater chironomid taxa a shift is apparent at ca. 37-30 cm depth where *M. radialis*-type and *Tanytarsus lugens/mendax*-type decline and Chironomus increases in percentages.

https://doi.org/10.5194/egusphere-2024-835
Preprint. Discussion started: 18 April 2024

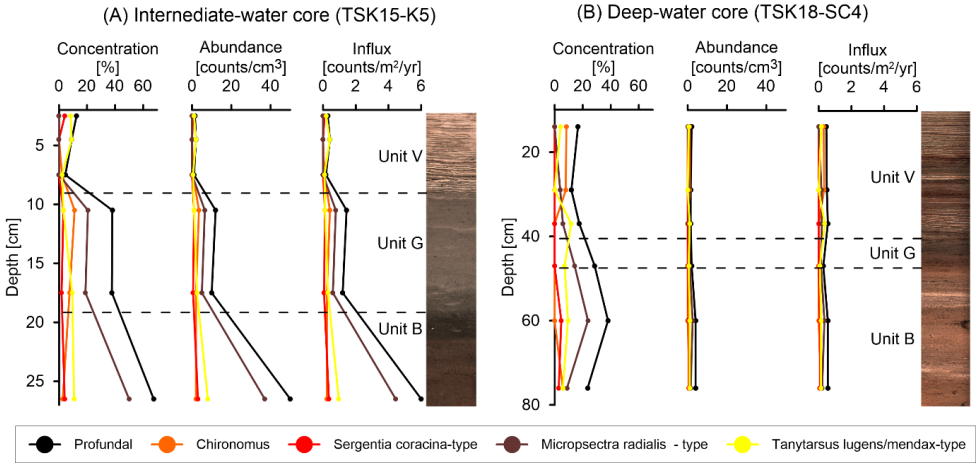

Figure 10. Abundances of chironomids, profundal chironomids, and selected profundal chironomid groups in cores TSK15-K5 (A) and in core TSK18-SC4 (B).

4.5 Limnological monitoring

The present-day DO dynamics are shown in lake monitoring data between April 2019 to February 2021 (Figure 11A) The dynamics of DO along the water column at the deepest part of the lake show clear seasonal fluctuations, in which DO at the upper ~12 m ranges from ~8 mg/l during the early spring to ~14 mg/l during the winter, while near the lakefloor, DO ranges from ~1 mg/l in early winter to ~11 mg/l during the spring. The depletion in DO at the hypolimnion first occurs at the water-sediment interface and progrades upward during the summer-autumn to a water depth of ~12 m (Figure 11A), which represents the oxycline. Thermal stratification prevails from April to November with an average thermocline depth of ~10 m (Figure 11B). The epilimnion temperature ranges from ~3 °C in winter to ~22 °C in summer, while hypolimnion temperature ranges from 3 °C in winter to 5 °C in summer. An interesting observation is the time shift between changes in the vertical oxygen distribution and the temperature dynamics. While the maximal temperature difference between the epi- and hypolimnion is achieved in August (Figure 11B), the maximal DO difference between the layers appears in November (Figure 11A).

https://doi.org/10.5194/egusphere-2024-835
Preprint. Discussion started: 18 April 2024

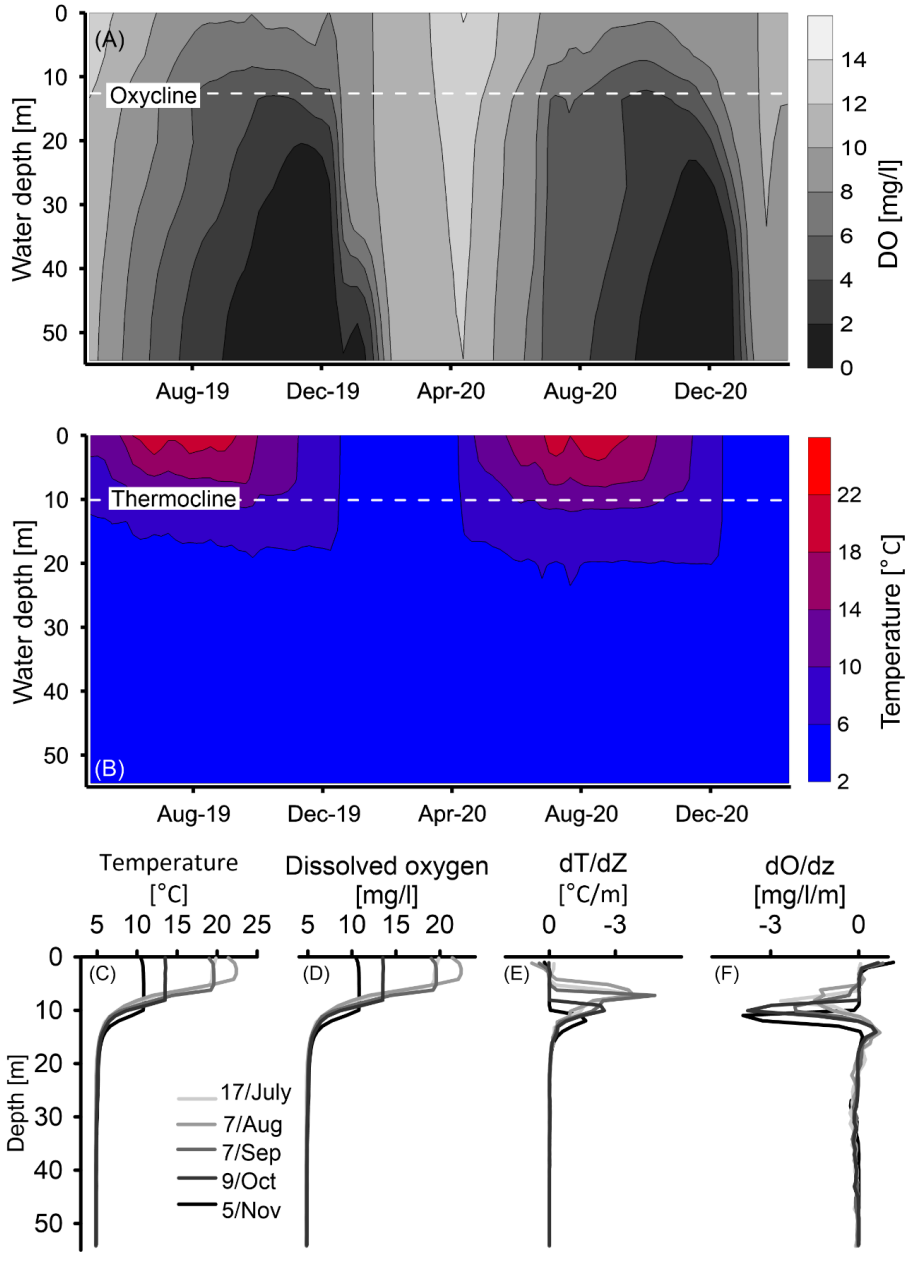

390 **Figure 11. Physical properties of the water column. Spatiotemporal characterization of dissolved oxygen (DO) (A) and temperature (B) in the lake. The diminishing of the temperature (C) and DO (D) stratification along the water column. The maximal depth gradient of temperature (E) and DO (F) along the water column show the evolution of the thermocline and oxycline depth.**

https://doi.org/10.5194/egusphere-2024-835
Preprint. Discussion started: 18 April 2024

5 Discussion

5.1 Present-day oxygen dynamics

The seasonal water column stratification and the associated lake circulation control the bottom water oxygenation in TSK. Present-day seasonal dynamics of DO concentrations in the lake show that hypoxia is extending upward in the water column during summer-autumn and is limited by the thermocline around 10 m depth (Figure 11). The vertical variations of DO along the water column at the deepest part of the lake allow to quantify the required intensity, duration and vertical development of hypoxia, which is required for varve preservation. The general definition for hypoxia is $[O_2] < 2\ \frac{mg}{l}$ (Diaz & Rosenberg, 1995; Jenny et al., 2014; Tyson & Pearson, 1991), although for freshwater lakes value of $[O_2] < 5\ \frac{mg}{l}$ have been used to define hypoxic conditions (Njiru et al., 2012). By adopting these numbers, we can define the hypoxic threshold for varve preservation at TSK below 12 m water depth by $[O_2] < 5\ \frac{mg}{l}$ for five months (August-December) and $[O_2] < 2\ \frac{mg}{l}$ for two months (November-December; Figure 11A). Our results show that in spite of the winter oxygenation of the water column, varves can be preserved in monomictic lakes, as long as the duration and magnitude of the seasonal hypoxia is sufficient. Only at the shallow lakefloor (<12 m) oxic conditions prevail during the entire year because the spread of hypoxia is limited by the thermocline. The time delay between the vertical oxygen distribution and temperature dynamics likely reflects the timing and duration of OM decomposition during the period of stratification at the deepest part of the lake basin and the circulation of lake water that starts from the bottom and the time required to transport oxygen into the bottom waters.

5.2 The transition from oxygenated to hypoxic conditions

The identification of the onset of varve preservation in the sedimentary record is a common tool to date the onset of hypoxic conditions in lakes because it indicates the absence of bioturbating organisms (e.g., Diaz and Rosenberg, 1995). However, varve preservation is a binary proxy that is only indicating a depletion of the DO level to below a certain threshold. To trace possible depletion in DO level prior to varve preservation, more sensitive geochemical proxies are applied. Geochemical sediment characterization by clustering of XRF data shows that the varved unit V, and the underlaying unit G are geochemically similar and reflect similar sediment composition (Figure 8). This is also supported by relative variations of endogenic calcite and detrital matter (Ca/Ti), and relative variations of biogenic silica and detrital matter (Si/Ti) (Figure 9). The increase of the $CaCO_3$ concentrations and Ca/Ti ratio at the transition from unit B to G, reflects an enhanced calcite formation (Figure 9). The increase in the Si/Ti records at the transition to unit G indicates a relative increase of diatom accumulation that continue into the varved unit V, but is less clear in the shallow core TSK23-SC2 located at a water depth of less than 12 m. Intervals of increasing calcite and diatom deposition are characterized by cluster 5 in shallow-water cores and cluster 4 in deep-water cores. Together, the rising deposition of calcite and diatom frustules indicate changes in sedimentation prior to the onset of varve preservation, while DO level were still sufficient for the existing of bioturbating organisms.

https://doi.org/10.5194/egusphere-2024-835
Preprint. Discussion started: 18 April 2024

Variations in Fe/Mn ratios are another sensitive proxy because oxidation of organic matter at the sediment-water interface and upper sediment is coupled to the reduction of Mn or Fe oxides. Decreasing Fe/Mn ratios at the transition from Unit B to G observed in all cores below 12 m water depth shows that redox processes are initiated at this depositional boundary (Figure 9). This suggests that the redox conditions at the sediment-water interface already changed prior to the onset of varve preservation. The bacterial oxidation of organic matter and reduction of Mn and Fe at the sediment-water interface are associated to changes in the DO level and related water circulation (Liu et al., 2022; Melton et al., 2014; Thamdrup, 2000). Relative constant Fe/Mn ratios in core TSK23-SC2 located above the oxycline (<12 m) does not show a decrease like in cores from locations with presently low DO levels and thus confirms the sensitivity of this proxy to oxygen conditions at the sediment-water interface. This is also supported by the upcore reduction in oxygen-sensitive chironomid abundance and the decrease in profundal chironomids already at the transition between Units B and G in core TSK15-K5. $\delta^{13}C_{org}$ profile of three cores (TSK11-K1, 62 m; TSK15-K5, 27.3 m; TSK23-SC2, 11.3 m) support the DO depletion in the deep part of the lake, while the shallower lakefloor remained oxygenated. $\delta^{13}C_{org}$ in the deep and intermediate cores show more negative values upcore, approaching $\delta^{13}C_{org}$ of recent organic materials from sediment traps, which experienced minor degradation (Supplementary material Figure S2). Those more negative $\delta^{13}C_{org}$ values are explained by less selective degradation and point to increasing organic matter preservation at the deep and intermediate lakefloor (Meyers, 1997; Spiker & Hatcher, 1987; Wynn, 2007). This indicates the onset of depletion in the DO level prior to the onset of varve preservation at the deep lakefloor, at the boundary between Units B and G. $\delta^{13}C_{org}$ values in the shallowest core are less negative and constant along the core (Figure 9C), reflecting oxygenating conditions for the last two centuries. This agrees with observation of DO dynamics in the lake, which show that the upper part of the water column, the top ~12 m, is oxygenated the whole year (Figure 11A).

The abundance of remains of chironomid larvae in two cores, from the deep and shallow parts of the lake basin, supports our hypothesis regarding DO depletion over time. Chironomids are oxygen-sensitive organisms (Brodersen et al., 2004; Heinis & Davids, 1993; Perret-Gentil et al., 2024; Ursenbacher et al., 2020) that can live in lacustrine deep-water environments. Of the deep-water chironomid groups identified in the sediments of Tiefer See, *M. radialis*-type is typically considered the most sensitive to eutrophication and associated oxygen decrease. Habitats with pronounced hypoxia over extended periods of time are usually characterized by an absence of deep-water chironomid larvae, low concentrations of chironomid remains and low absolute abundances and percentages of profundal chironomid groups in subfossil chironomid assemblages (Brodersen & Quinlan, 2006; Ursenbacher et al., 2020; Van Hardenbroek et al., 2011). Chironomid remains in core TSK15-K5 from intermediate water depth support the two-step DO depletion in the lake as high concentrations and influx values of total and profundal chironomids were observed in Unit B, lower abundances in the Unit G and negligible abundance in Unit V (Figure 10). This decrease in DO is also confirmed by the distinct reduction in *M. radialis*-type, the dominant deep-water taxon in the core (Figure 10). The overall low concentrations, influx values and percentages of profundal chironomids in the deep-water core TSK18-SC4 may indicate that during the entire studied interval the deep-water core was characterized by lower DO levels compared to the intermediate core. This indicates that relatively low DO levels in the depocenter of the lake prevailed even

https://doi.org/10.5194/egusphere-2024-835
Preprint. Discussion started: 18 April 2024

during the deposition of unit B, which is considered to reflect the most oxygenated conditions. However, the DO level at the time was insufficient for varve preservation and only a further decrease in the DO resulted in the preservation of varves in the depocenter from the base of Unit V onwards.

In summary, the transition from units B to G marks a change in the geochemical composition of the sediments driven by initial DO depletion at the lakefloor prior to the onset of varve preservation. Therefore, the onset of varve preservation reflects a threshold in DO level and duration of hypoxia required for varve preservation. The time difference between the onset of DO depletion and the onset of varve preservation provides an estimate of the sensitivity of the lake system to environmental change.

5.3 Time shift between the onset of oxygen depletion and varve preservation

The time the onset of geochemical changes (B-G boundary) and the onset of varve preservation (G-V boundary) is determined through the Askja-1875 cryptotephra at the transition between Units B and G and the varve-dated onset of annual laminations at the different locations and ranges from ~15 yrs in the depocenter (62 m) to ~80-100 yrs at intermediate water depths (27-35 m) (Figure 12). This difference implies that the cessation of bioturbation is more rapid in the depocenter compared to intermediate water depths. The faster sediment response at the depocenter to depleting DO levels can be explained by the following mechanism: (i) The depocenter experienced higher TOC flux and thus enhanced OM decomposition and DO depletion. (ii) At intermediate water depths DO levels sufficiently low to allow varve preservation were reached later because water column mixing and circulation have more influence on DO levels than on the deep lakefloor.

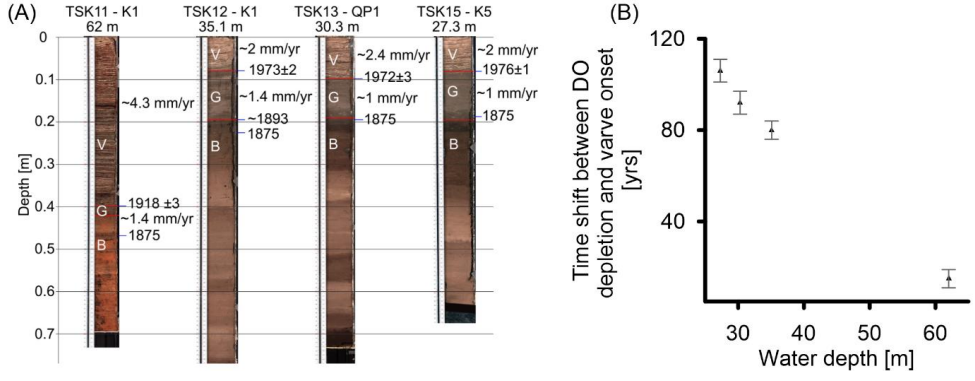

Figure 12. (A) Images of the selected cores and their chronologic anchors. (B) The time interval between the onset of DO depletion (base of Unit G) and the onset of varve preservation (base of Unit V).

5.4 Basin scale spread of hypoxia

To discuss the basin-wide spread of hypoxia, we use the onset of varve preservation as a proxy for hypoxia because this is best visible in the core and comparable with other studies based on this indicator (e.g., Jenny et al., 2016), keeping in mind, however, that DO depletion started a few decades earlier. It took ~80 yr from crossing the DO threshold at 62 m water depth (CE 1918±1) until it reached 16 m water depth in CE 1997±1

https://doi.org/10.5194/egusphere-2024-835
Preprint. Discussion started: 18 April 2024

(Figure 6). A similar rate of hypoxia spread in two phases is observed in two morphometric variables, (i) the lakefloor area, and (ii) the water volume (Figure 13). In the first phase, from 1918 and 1972, the rate in which the lakefloor becomes hypoxic was $1 - 3.5 \cdot 10^3\ m^2/yr$, and the rate of water volume that becomes hypoxic was $10 - 35 \cdot 10^3\ m^3/yr$. In the second phase between 1972 and 1997 these rates increased substantially reaching a rate of $10 - 14 \cdot 10^3\ m^2/yr$ for the spread of hypoxia on the lakefloor, and $138 - 164 \cdot 10^3\ m^3/yr$ of water volume that became hypoxic. Moreover, between 1918 and 1997, the proportion of the lakefloor area that experienced hypoxic conditions increased to 52% of the total lakefloor (Figure 13C, brown dots), while the water volume that became hypoxic increased only to 36% of the total water volume (Figure 13C, blue dots). This yields an increasing difference between the percentage of hypoxic lakefloor area and water volume hypoxia over time as at any water depth, the proportion of the lakefloor that is hypoxic is larger than the proportion of the water volume. The acceleration in the rate of hypoxia spread in TSK around CE 1972 is controlled by the shape of the basin and occurred when the level of hypoxia reached a water depth of ~30 m, equal to the slope break (Figure 1C). At that point, the rate in which the lakefloor and the water volume became hypoxic increased by almost an order of magnitude.

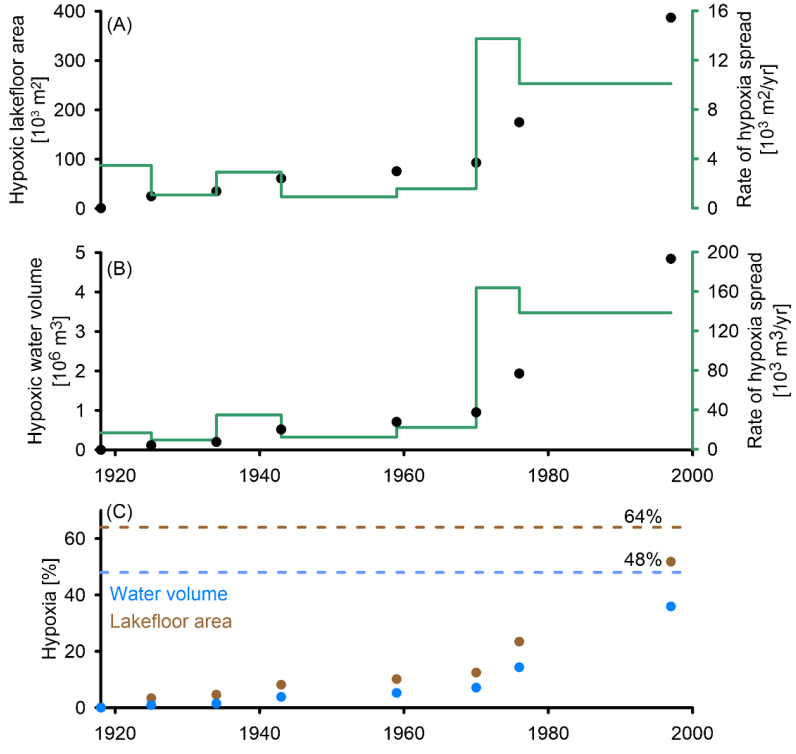

Figure 13. The spread of hypoxia in the lake (black) and its rate (green) over time. (A) The rate in which the lakefloor becomes hypoxic. (B) The rate in which the lake's water volume becomes hypoxic. (C) Percentage of hypoxic water volume (blue dots) and lakefloor area (brown dots) from the total. The dashed lines indicate the maximal extent of hypoxia under present-day conditions, when the seasonal oxycline is at ~12 m depth.

https://doi.org/10.5194/egusphere-2024-835
Preprint. Discussion started: 18 April 2024

6 Conclusions

The depletion of DO in the TSK during the past two centuries is recorded by varve microfacies and geochemical and biological proxies and revealed the presence of several threshold processes.

1. Preservation of varves marks a depletion of DO level to below a threshold of $[O_2] < 5$ mg/l for five months and $[O_2] < 2$ mg/l for two months under seasonal hypoxic conditions. This provides evidence that the presence of varves not necessarily requires meromictic conditions (permanent stratification).

2. According to changes in sediment geochemistry oxygen levels initially decreased around CE 1875 and continued for another four to five decades until at the depocenter of the lake a threshold in oxygen depletion was crossed allowing varve to be preserved.

3. Hypoxic conditions sufficient to allow varve preservation spread upwards in the lake basin during ~80 years from the deepest part of the lake up to a water depth of 16 m. The upper limit of hypoxic conditions is defined by the oxycline, roughly reflecting the thermocline, above which permanent oxygenated conditions prevail and no varves are present.

4. The basin morphology controls the spread of hypoxia which occurred in two phases. An acceleration occurred during the 1970s when the level of hypoxia reached the slope break at ~30 m.

5. The biogeochemical cycles in the lake reflected in calcite, diatom production and TOC deposition intensified along with the development of hypoxic conditions.

Data availability

All raw data can be provided by the corresponding authors upon request.

Author contribution

IS – conceptualization, data curation, investigation, funding acquisition, visualization, writing - original draft. RT - data curation, formal analysis, visualization, software, writing - review & editing. SP - data curation, writing - review & editing. BS - data curation, writing - review & editing. MA - data curation. RK - data curation. OH - data curation, visualization, writing - review & editing. SB - data curation, visualization, writing - review & editing. AB – conceptualization, investigation, funding acquisition, Project administration, writing - review & editing.

Competing interests

The authors declare that they have no conflict of interest.

7 Acknowledgements

Brian Brademann and Karla Wurz are thanked for the assistance in field and lab work. IS was supported by a post-doctoral fellowship from the Alexander Von Humboldt foundation. The monitoring equipment used in this study was funded by the Terrestrial Environmental Observatory Infrastructure initiative of the Helmholtz

https://doi.org/10.5194/egusphere-2024-835
Preprint. Discussion started: 18 April 2024

Association (TERENO Observatory NE Germany). It is further a contribution to the Helmholtz climate initiative REKLIM (Regional Climate Change and Humans) 'Research Theme 3 Extreme events across temporal and spatial scales'.

References

Anderson, R. Y., & Dean, W. E. (1988). Lacustrine varve formation through time. *Palaeogeography, Palaeoclimatology, Palaeoecology, 62*(`1-4), 215-235.

Arthur, M. A., & Dean, W. E. (1998). Organic-matter production and preservation and evolution of anoxia in the Holocene Black Sea. *Paleoceanography, 13*(4), 395-411.

Benner, R., Fogel, M. L., Sprague, E. K., & Hodson, R. E. (1987). Depletion of 13C in lignin and its implications for stable carbon isotope studies. *Nature, 329*(6141), 708-710.

Blockley, S. P., Pyne-O'Donnell, S. D., Lowe, J. J., Matthews, I. P., Stone, A., Pollard, A. M., et al. (2005). A new and less destructive laboratory procedure for the physical separation of distal glass tephra shards from sediments. *Quaternary Science Reviews, 24*(16-17), 1952-1960.

Brauer, A., & Casanova, J. (2001). Chronology and depositional processes of the laminated sediment record from Lac d'Annecy, French Alps. *Journal of Paleolimnology, 25*, 163–177.

Brodersen, K. P., Pedersen, O., Lindegaard, C., & Hamburger, K. (2004). Chironomids (Diptera) and oxy-regulatory capacity: an experimental approach to paleolimnological interpretation. *Limnology and Oceanography, 49*(5), 1549-1559.

Brodersen, K. P., & Quinlan, R. (2006). Midges as palaeoindicators of lake productivity, eutrophication and hypolimnetic oxygen. *Quaternary Science Reviews, 25*(15-16), 1995-2012.

Brooks, S. J., Langdon, P. G., & Heiri, O. (2007). The identification and use of Palaearctic Chironomidae larvae in palaeoecology. Retrieved from

Buatois, L. A., Renaut, R. W., Owen, R. B., Behrensmeyer, A. K., & Scott, J. J. (2020). Animal bioturbation preserved in Pleistocene magadiite at Lake Magadi, Kenya Rift Valley, and its implications for the depositional environment of bedded magadiite. *Scientific Reports, 10*(1).

Davies, B. R. (1976). The dispersal of Chironomidae larvae: a review. *Journal of the Entomological Society of Southern Africa, 39*(1), 39-62.

Dean, W. E., & Gorham, E. (1998). Magnitude and significance of carbon burial in lakes, reservoirs, and peatlands. *Geology, 26*(6), 535-538.

Diaz, R. J., & Rosenberg, R. (1995). Marine benthic hypoxia: A review of its ecological effects and the behavioural response of benthic macrofauna. *Oceanography and marine biology: An annual review, 33*, 245-303.

https://doi.org/10.5194/egusphere-2024-835
Preprint. Discussion started: 18 April 2024

Diaz, R. J., & Rosenberg, R. (2008). Spreading dead zones and consequences for marine ecosystems. *Science, 321*(5891), 926-929.

Dräger, N., Plessen, B., Kienel, U., Słowinski, M., Ramisch, A., Tjallingii, R., et al. (2019). Hypolimnetic oxygen conditions influence varve preservation and d13C of sediment organic matter in Lake Tiefer See, NE Germany. *Journal of Paleolimnology, 62*, 181–194-181–194.

Dräger, N., Theuerkauf, M., Szeroczyńska, K., Wulf, S., Tjallingii, R., Plessen, B., et al. (2017). Varve microfacies and varve preservation record of climate change and human impact for the last 6000 years at Lake Tiefer See (NE Germany). *The Holocene, 27*(3), 450– 464-450– 464.

Evans, G., Augustinus, P., Gadd, P., Zawadzki, A., & Ditchfield, A. (2019). A multi-proxy µ-XRF inferred lake sediment record of environmental change spanning the last ca. 2230 years from Lake Kanono, Northland, New Zealand. *Quaternary Science Reviews, 225*.

Friedrich, J., Janssen, F., Aleynik, D., Bange, H. W., Boltacheva, N., Çagatay, M. N., & Wenzhöfer, F. (2014). Investigating hypoxia in aquatic environments: diverse approaches to addressing a complex phenomenon. *Biogeosciences, 11*(4), 1215-1259.

He, W., You, L., Chen, M., Tuo, Y., Liao, N., Wang, H., & Li, J. (2023). Varied sediment archive of Fe and Mn contents under changing reservoir mixing patterns, oxygenation regimes, and runoff inputs. *Ecological Indicators, 147*(109967).

Heinis, F., & Davids, C. (1993). Factors governing the spatial and temporal distribution of chironomid larvae in the Maarsseveen lakes with special emphasis on the role of oxygen conditions. *Netherland Journal of Aquatic Ecology, 27*, 21-34.

Hunt, J. B., & Hill, P. G. (1996). An inter-laboratory comparison of the electron probe microanalysis of glass geochemistry. *Quaternary International, 34*, 229-241.

Jankowski, T., Livingstone, D. M., Bührer, H., Forster, R., & Niederhauser, P. (2006). Consequences of the 2003 European heat wave for lake temperature profiles, thermal stability, and hypolimnetic oxygen depletion: Implications for a warmer world. *Limnology and Oceanography, 51*(2), 815-819.

Jenny, J. P., Arnaud, F., Alric, B., Dorioz, J. M., Sabatier, P., Meybeck, M., & Perga, M. E. (2014). Inherited hypoxia: A new challenge for reoligotrophicated lakes under global warming. *Global Biogeochemical Cycles, 28*(12), 1413-1423.

Jenny, J. P., Arnaud, F., Dorioz, J. M., Giguet Covex, C., Frossard, V., Sabatier, P., et al. (2013). A spatiotemporal investigation of varved sediments highlights the dynamics of hypolimnetic hypoxia in a large hard-water lake over the last 150 years. *Limnology and Oceanography, 58*(4), 1395-1408.

Jenny, J. P., Francus, P., Normandeau, A., Lapointe, F., Perga, M. E., Ojala, A., et al. (2016). Global spread of hypoxia in freshwater ecosystems during the last three centuries is caused by rising local human pressure. *Global Change Biology, 22*(4), 1481-1489.

https://doi.org/10.5194/egusphere-2024-835
Preprint. Discussion started: 18 April 2024

Jochum, K. P., Stoll, B., Herwig, K., Willbold, M., Hofmann, A. W., Amini, M., et al. (2006). MPI-DING reference glasses for in situ microanalysis: New reference values for element concentrations and isotope ratios. *Geochemistry, Geophysics, Geosystems, 7*(2).

Kastowski, M., Hinderer, M., & Vecsei, A. (2011). Long-term carbon burial in European lakes: Analysis and estimate. *Global Biogeochemical Cycles, 25*(3).

Kelts, K., & Hsü, K. J. (1978). Freshwater Carbonate Sedimentation. In A. Lerman (Ed.), *Freshwater carbonate sedimentation. In Lakes: chemistry, geology, physics* (pp. 295-323). New York, NY: Springer New York.

Kienel, U., Dulski, P., Ott, F., Lorenz, S., & Brauer, A. (2013). Recently induced anoxia leading to the preservation of seasonal laminae in two NE-German lakes. *Journal of Paleolimnology, 50*(4), 535-544.

Kienel, U., Kirillin, G., Brademann, B., Plessen, B., Lampe, R., & Brauer, A. (2017). Effects of spring warming and mixing duration on diatom deposition in deep Tiefer See, NE Germany. *Journal of Paleolimnology, 57*(1), 37-49.

Lane, C. S., Cullen, V. L., White, D., Bramham-Law, C. W. F., & Smith, V. C. (2014). Cryptotephra as a dating and correlation tool in archaeology. *Journal of Archaeological Science, 42*, 42-50.

Lehmann, M. F., Bernasconi, S. M., Barbieri, A., & McKenzie, J. A. (2002). Preservation of organic matter and alteration of its carbon and nitrogen isotope composition during simulated and in situ early sedimentary diagenesis. *Geochimica et Cosmochimica Acta, 66*(20), 3573-3584.

Liu, J., Chen, Q., Yang, Y., Wei, H., Laipan, M., Zhu, R., et al. (2022). Coupled redox cycling of Fe and Mn in the environment: The complex interplay of solution species with Fe-and Mn-(oxyhydr) oxide crystallization and transformation. *Earth-Science Reviews, 232*(104105).

Loizeau, J. L., Span, D., Coppee, V., & Dominik, J. (2001). Evolution of the trophic state of Lake Annecy (eastern France) since the last glaciation as indicated by iron, manganese and phosphorus speciation. *Journal of Paleolimnology, 25*, 205-214.

Makri, S., Rey, F., Gobet, E., Gilli, A., Tinner, W., & Grosjean, M. (2020). Early human impact in a 15,000-year high-resolution hyperspectral imaging record of paleoproduction and anoxia from a varved lake in Switzerland. *Quaternary Science Reviews, 239*.

Makri, S., Wienhues, G., Bigalke, M., Gilli, A., Rey, F., Tinner, W., & Grosjean, M. (2021). Variations of sedimentary Fe and Mn fractions under changing lake mixing regimes, oxygenation and land surface processes during Late-glacial and Holocene times. *Science of the Total Environment, 755*(143418).

Meire, L., Soetaert, K. E. R., & Meysman, F. J. R. (2013). Impact of global change on coastal oxygen dynamics and risk of hypoxia. *Biogeosciences, 10*(4), 2633-2653.

Melton, E. D., Swanner, E. D., Behrens, S., Schmidt, C., & Kappler, A. (2014). The interplay of microbially mediated and abiotic reactions in the biogeochemical Fe cycle. *Nature Reviews Microbiology, 12*(12), 797-808.

https://doi.org/10.5194/egusphere-2024-835
Preprint. Discussion started: 18 April 2024

Mendonça, R., Müller, R. A., Clow, D., Verpoorter, C., Raymond, P., Tranvik, L. J., & Sobek, S. (2017). Organic carbon burial in global lakes and reservoirs. *Nature Communications, 8*(1), 1694.

Meyers, P. A. (1997). Organic geochemical proxies of paleoceanographic, paleolimnologic, and paleoclimatic processes. *Organic geochemistry, 27*(5-6), 213-250.

Mollenhauer, G., & Eglinton, T. I. (2007). Diagenetic and sedimentological controls on the composition of organic matter preserved in California Borderland Basin sediments. *Limnology and Oceanography, 52*(2), 558-576.

Mulholland, P. J., & Elwood, J. W. (1982). The role of lake and reservoir sediments as sinks in the perturbed global carbon cycle. *Tellus, 34*(5), 490-499.

Njiru, M., Nyamweya, C., Gichuki, J., Mugidde, R., Mkumbo, O., & Witte, F. (2012). Increase in anoxia in Lake Victoria and its effects on the fishery. In P. Padilla (Ed.), *Anoxia* (pp. 99-128).

Nürnberg, G. K. (2004). Quantified Hypoxia and Anoxia in Lakes and Reservoirs. *The Scientific World Journal, 4*, 42–54.

O'Reilly, C. M., Sharma, S., Gray, D. K., Hampton, S. E., Read, J. S., Rowley, R. J., et al. (2015). Rapid and highly variable warming of lake surface waters around the globe. *Geophysical Research Letters, 42*(24), 10773-10781.

Ojala, A. E., Saarinen, T., & Salonen, V. P. (2000). Preconditions for the formation of annually laminated lake sediments in southern and central Finland. *Boreal Environment Research, 5*(3), 243-255.

Perret-Gentil, N., Rey, F., Gobet, E., Tinner, W., & Heiri, O. (2024). Human impact leads to unexpected oligotrophication and deepwater oxygen increase in a Swiss mountain lake. *The Holocene, 34*(2), 189–201.

Roeser, P., Drager, N., Dariusz, B., Ott, F., Pinkerneil, S., Gierszewski, P., et al. (2021). Advances in understanding calcite varve formation : new insights from a dual lake monitoring approach in the southern Baltic lowlands. *Boreas*.

Saether, O. A. (1979). Chironomid communities as water quality indicators. *Ecography, 2*(2), 65-74.

Sanchini, A., Szidat, S., Tylmann, W., Vogel, H., Wacnik, A., & Grosjean, M. (2020). A Holocene high-resolution record of aquatic productivity, seasonal anoxia and meromixis from varved sediments of Lake Łazduny, North-Eastern Poland: insight from a novel multi-proxy approach. *Journal of Quaternary Science, 35*(8), 1070-1080.

Schaffner, L. C., Jonsson, P., Diaz, R. J., Rosenberg, R., & Gapcynski, P. (1992). *Benthic communities and bioturbation history of estuarine and coastal systems: effects of hypoxia and anoxia.* Paper presented at the Marine Coastal Eutrophication.

Shatkay, M., Anati, D. A., & Gat, J. R. (1993). Dissolved oxygen in the Dead Sea - seasonal changes during the holomictic stage. *International Journal of Salt Lake Research, 2*(95), 93-110.

https://doi.org/10.5194/egusphere-2024-835
Preprint. Discussion started: 18 April 2024

Sobek, S., Durisch-Kaiser, E., Zurbrügg, R., Wongfun, N., Wessels, M., Pasche, N., & Wehrli, B. (2009). Organic carbon burial efficiency in lake sediments controlled by oxygen exposure time and sediment source. *Limnology and Oceanography*, *54*(6), 2243-2254.

Sorrel, P., Jacq, K., Van Exem, A., Escarguel, G., Dietre, B., Debret, M., & Oberhänsli, H. (2021). Evidence for centennial-scale Mid-Holocene episodes of hypolimnetic anoxia in a high-altitude lake system from central Tian Shan (Kyrgyzstan). *Quaternary Science Reviews*, *252*(106748).

Spiker, E. C., & Hatcher, P. G. (1987). The effects of early diagenesis on the chemical and stable carbon isotopic composition of wood. *Geochimica et Cosmochimica Acta*, *51*(6), 1385-1391.

Steinsberger, T., Schmid, M., Wüest, A., Schwefel, R., Wehrli, B., & Müller, B. (2017). Organic carbon mass accumulation rate regulates the flux of reduced substances from the sediments of deep lakes. *Biogeosciences*, *14*(13), 3275-3285.

Straile, D., Jöhnk, K., & Rossknecht, H. (2003). Complex effects of winter warming on the physicochemical characteristics of a deep lake. *Limnology and Oceanography*, *48*(4), 1432-1438.

Teranes, J. L., & Bernasconi, S. M. (2005). Factors controlling δ13C values of sedimentary carbon in hypertrophic Baldeggersee, Switzerland, and implications for interpreting isotope excursions in lake sedimentary records. *Limnology and Oceanography*, *50*(3), 914-922.

Thamdrup, B. (2000). Bacterial manganese and iron reduction in aquatic sediments. In *Advances in microbial ecology* (pp. 41-84). Boston: Springer.

Tjallingii, R., Röhl, U., Kölling, M., & Bickert, T. (2007). Influence of the water content on X-ray fluorescence core-scanning measurements in soft marine sediments. *Geochemistry, Geophysics, Geosystems*, *8*(2).

Tranvik, L. J., Downing, J. A., Cotner, J. B., Loiselle, S. A., Striegl, R. G., Ballatore, T. J., & Weyhenmeyer, G. A. (2009). Lakes and reservoirs as regulators of carbon cycling and climate. *Limnology and Oceanography*, *54*(6), 2298-2314.

Tylmann, W., Szpakowska, K., Ohlendorf, C., Woszczyk, M., & Zolitschka, B. (2012). Conditions for deposition of annually laminated sediments in small meromictic lakes: A case study of Lake Suminko (Northern Poland). *Journal of Paleolimnology*, *47*(1), 55-70.

Tyson, R. V., & Pearson, T. H. (1991). Modern and ancient continental shelf anoxia: an overview. *Geological Society, London, Special Publications*, *58*(1), 1-24.

Ursenbacher, S., Stötter, T., & Heiri, O. (2020). Chitinous aquatic invertebrate assemblages in Quaternary lake sediments as indicators of past deepwater oxygen concentration. *Quaternary Science Reviews*, *231*(106203).

Van Hardenbroek, M., Heiri, O., Wilhelm, M. F., & Lotter, A. F. (2011). How representative are subfossil assemblages of Chironomidae and common benthic invertebrates for the living fauna of Lake De Waay, the Netherlands? *Aquatic Sciences*, *73*, 247-259.

https://doi.org/10.5194/egusphere-2024-835
Preprint. Discussion started: 18 April 2024

Vaquer-Sunyer, R., & Duarte, C. M. (2008). Thresholds of hypoxia for marine biodiversity. *Proceedings of the National Academy of Sciences, 105*(40), 15452-15457.

Weltje, G. J., Bloemsma, M. R., Tjallingii, R., Heslop, D., Röhl, U., & Croudace, I. W. (2015). Prediction of geochemical composition from XRF core scanner data: a new multivariate approach including automatic selection of calibration samples and quantification of uncertainties. In *Micro-XRF Studies of Sediment Cores: Applications of a non-destructive tool for the environmental sciences* (pp. 507-534).

Wetzel, R. G. (2001). *Limnology: lake and river ecosystems* (third ed.): Elsevier.

Wiederholm, T. (1983). Chironomidae of the holarctic region. Keys and diagnoses. Part 1: larva. In *Ent Scand Suppl* (Vol. 19, pp. 1-457).

Wulf, S., Dräger, N., Ott, F., Serb, J., Appelt, O., Guðmundsdóttir, E., et al. (2016). Holocene tephrostratigraphy of varved sediment records from Lakes Tiefer See (NE Germany) and Czechowskie (N Poland). *Quaternary Science Reviews, 132*, 1-14.

Wynn, J. G. (2007). Carbon isotope fractionation during decomposition of organic matter in soils and paleosols: Implications for paleoecological interpretations of paleosols. *Palaeogeography, Palaeoclimatology, Palaeoecology, 251*, 437–448.

Zander, P. D., Żarczyński, M., Vogel, H., Tylmann, W., Wacnik, A., Sanchini, A., & Grosjean, M. (2021). A high-resolution record of Holocene primary productivity and water-column mixing from the varved sediments of Lake Żabińskie, Poland. *Science of the Total Environment, 755*(143713).

Żarczyński, M., Wacnik, A., & Tylmann, W. (2019). Tracing lake mixing and oxygenation regime using the Fe/Mn ratio in varved sediments: 2000 year-long record of human-induced changes from Lake Żabińskie (NE Poland). *Science of the Total Environment, 657*, 585-596.

Zolitschka, B., Francus, P., Ojala, A. E. K., & Schimmelmann, A. (2015). Varves in lake sediments - a review. *Quaternary Science Reviews, 117*, 1-41. http://dx.doi.org/10.1016/j.quascirev.2015.03.019